Perturbation of eddy-currents by one inclusion in liquid metal

Rafaël Guichou, Hervé Ayroles, Rémi Zamansky, Wladimir Bergez, Philippe Tordjeman, Kevin Paumel

Perturbation of eddy-currents by one inclusion in liquid metal

doi: 10.1063/1.5055062

R. Guichou,[1] H. Ayroles,[1] R. Zamansky,[1] W. Bergez,[1] Ph. Tordjeman,[1] and K. Paumel[2]

AFFILIATIONS

[1]Institut de Mécanique des Fluides de Toulouse (IMFT), Université de Toulouse, CNRS, Toulouse, France
[2]Nuclear Technology Department, CEA, DEN, F-13108 Saint Paul Lez Durance, France

ABSTRACT

In this article, we present an analytical model to calculate the perturbation of the magnetic vector potential due to a non-conducting inclusion in a liquid metal translated at constant velocity. The model is valid for a low magnetic Reynolds number, Re_m, and a low shielding parameter, S_ω. We establish that the first order perturbation of the vector potential can be directly obtained from the value of the unperturbed eddy-current calculated at the location of the inclusion. An ECFM (Eddy-Current FlowMeter) device has been designed to validate the model and to study the frequency effects of the eddy-current and the volume of one inclusion and its location. We observe a good agreement between the model predictions and experimental data within the limit of the validity of the model. Based on scaling analysis, we show that a unique relation exists between the perturbation of the emf (electromotive force) measured with the ECFM and the volume of the inclusion and its location, which reflects the self-similarity of the model solution.

https://doi.org/10.1063/1.5055062

I. INTRODUCTION

When a flow of electrically conducting liquid undergoes an AC magnetic field, the presence of non-conducting inclusions modifies the electric current distribution. Understanding, predicting, and experimenting the distribution of the induced currents is important for fundamental magnetohydrodynamics and geophysics and is a key issue in many manufacturing processes or nuclear industry.[1–4] In this article, we propose a theoretical model of the perturbed magnetic vector potential caused by the distortion of eddy-currents around an inclusion immersed in a liquid metal flow. For a small magnetic Reynolds number, $Re_m = \mu_0\sigma_0 UL$ (where μ_0, σ_0, and U are the magnetic permeability of the vacuum, the electrical conductivity, and the velocity of the liquid, respectively, and L is the length scale of the flow), this model predicts the effects of the main physical parameters, such as the location and size of the inclusion, the frequency, and the electrical properties of the liquid metal. The model is compared and agrees very well with experiments and shows that the location and the volume of the inclusion determine the perturbation of the vector potential through an explicit relation.

Maxwell first developed a multipolar model to characterize the equivalent electrical conductivity of a two-phase medium composed of a conducting continuum phase containing a dispersion of non-conducting spherical inclusions.[5] This model is valid for DC electromagnetic fields but is not adapted to experiments in AC fields.[4] The main theoretical approach that takes into account the Faraday induction is due to Bowler who has modeled the electric field in a medium containing a flaw of different conductivity.[6] The model is based on the Green function method and requires a numerical modelling to solve a Fredholm integral equation for the current density perturbation. This model predicts correctly the location and the size of surface defects. Furthermore, the hydrodynamics of a liquid metal flow with inclusions requires the coupled resolution of the Maxwell and the Navier-Stokes equations. In the case of the DC magnetic field, direct numerical simulations showed that the Lorentz force significantly modifies the wake and the inclusion dynamics.[7,8] Finally, recent experimental studies show that the presence of a particle can be detected with a permanent magnet by the so-called Lorentz force velocimetry technique.[9] In this paper, we focus on the magnetic field perturbation by a liquid flow with a single inclusion in an AC external field. The paper is organized as follows: the model is presented in Sec. II and the experimental setup that has been designed to explore the validity range of the model is depicted in Sec. III. Then, the results are presented and discussed in Sec. IV.

II. PERTURBATION MODEL

We consider a model of a liquid metal flow in a cylindrical duct that advects one non-conducting spherical inclusion of radius

R_b (Fig. 1). The present model is based on the determination of the magnetic vector potential, $\mathbf{A}$, in the presence of the inclusion. The electromagnetic field is generated by an external primary coil P supplied with AC current I^e, corresponding to a volume current density $\mathbf{j^e}$. The perturbation of $\mathbf{A}$ is responsible for the difference of the magnetic flux through the secondary coils S1 and S2 when the liquid metal is flowing through the three coils. The device based on these principles is currently used to measure the flow rate and is called ECFM (Eddy-Current FlowMeter).[10]

In the model, we assume that the velocity field of the liquid metal is not perturbed by the magnetic field. Indeed, the magnetic interaction number is lower than unity due to a small advective time (Reynolds number > 1000), a hypothesis that is confirmed by previous experiments.[4] For the gauge $\nabla \cdot \mathbf{A} = 0$, the induction equation for the non-dimensional vector potential is

$$\nabla^2 \mathbf{A} = nS_\omega \frac{\partial \mathbf{A}}{\partial t} - nRe_m \mathbf{u} \times \nabla \times \mathbf{A} - \mathbf{j}^e, \tag{1}$$

where $n = 1_{LM}(\mathbf{r})$ is the characteristic function of the liquid metal volume ($n = 1$ in the liquid metal and 0 outside of the duct and in the inclusion). Note that the current density $\mathbf{j}^e$ is non-zero in the primary coil P only. In Eq. (1), the scalar potential gradient is neglected because of the absence of applied potential on the boundaries and $Re_m \ll 1$. The characteristic time is ω^{-1}, the inverse of the electrical current pulsation. The scale factor for $\mathbf{A}$ is also defined as $\mu_0 J^e L^2$, where J^e is the amplitude of the external current density. The shielding parameter $S_\omega = \mu_0 \sigma_0 \omega L^2$ corresponds to the square ratio of L and the magnetic skin depth.[11] Note that the first two terms on the right-hand side of Eq. (1) correspond to magnetic induction by Faraday and velocity effects.

In the absence of inclusion, the unperturbed vector potential amplitude $\mathbf{A}_0$ defines the "base" field for the liquid metal and obeys the same equation (1). For the geometry considered in this model with a uniform axial velocity, $\mathbf{A}_0$ is orthoradial. The solution of Eq. (1) is obtained from the Green function method as

$$\mathbf{A_0}(\mathbf{r}) = \int_{V_P} G(\mathbf{r}, \mathbf{r}') \mathbf{j}^e(\mathbf{r}') dV(\mathbf{r}'), \tag{2}$$

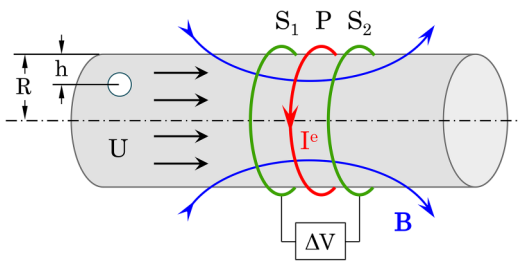

FIG. 1. Non-conducting inclusion advected by a flowing liquid metal and detected by an Eddy-Current FlowMeter (ECFM): P is the primary coil excited by an AC current I^e. S1 and S2 are two secondary coils, and U is the velocity of the liquid metal flow. The magnetic flux is measured with S1 and S2.

where V_P is the volume of the primary coil P and $G(\mathbf{r}, \mathbf{r}')$ is the scalar Green function given by[12,13]

$$G(\mathbf{r}, \mathbf{r}') = \int_{-\infty}^{+\infty} [C_i(r') I_1(k_i r) + D_i(r') K_1(k_i r)] \; e^{j2\pi\zeta(z-z')} d\zeta. \tag{3}$$

In this equation, the i index corresponds to three different domains: $i = 1$ for the liquid metal, $i = 2$ for the gap between the liquid and the coils, and $i = 3$ for the region external to the coils. We define $k_i^2 = (2\pi\zeta)^2 + j(2\pi\zeta Re_m + S_\omega)$ for $i = 1$ and $k_i^2 = (2\pi\zeta)^2$ for $i = 2, 3$. In Eq. (3), the position is given in cylindrical coordinates with the origin at the P coil center. The constants C_i and D_i are determined from the jump conditions: $[G(\mathbf{r}, \mathbf{r}')]_i^{i+1} = 0$, $\left[\frac{\partial G(\mathbf{r}, \mathbf{r}')}{\partial r}\right]_i^{i+1} = 0$, for $i = 1, 2$, except for the z position of the Dirac source where $\left[\frac{\partial G(\mathbf{r}, \mathbf{r}')}{\partial r}\right]_2^3 = 1$. In Eq. (3), I_1 and K_1 are the modified Bessel functions.[14] Note that the induction in the metal, characterized by the imaginary part in k_1, is responsible for a phase shift between $\mathbf{A}_0$ and the reference $\mathbf{j}^e$.

In the presence of one advected inclusion located at a distance h from the duct wall, the vector potential perturbation is $\mathbf{A}_\alpha = \mathbf{A} - \mathbf{A}_0$. For standard experimental conditions, the advection time is much larger than ω^{-1}, which implies $Re_m \ll S_\omega$. Based on this scale separation, the time derivative in Eq. (1) corresponds to the fast variations at the scale ω^{-1}. Consequently, $\mathbf{A}_\alpha$ obeys at first order in Re_m to the following equation:

$$\nabla^2 \mathbf{A}_\alpha \approx nS_\omega \frac{\partial \mathbf{A}_\alpha}{\partial t} - n_b S_\omega \frac{\partial \mathbf{A}_0}{\partial t}, \tag{4}$$

where $n_b = 1_b(\mathbf{r})$ is the characteristic function associated with the inclusion volume V_b. For a characteristic length $L = R_b$, which is small when compared with the skin depth, $S_\omega \ll 1$, and considering the expansion $\mathbf{A}_\alpha = S_\omega \mathbf{A}_\alpha^1 + S_\omega^2 \mathbf{A}_\alpha^2 + \cdots$, Eq. (4) leads to a Poisson equation

$$\nabla^2 \mathbf{A}_\alpha^1 = -n_b \frac{\partial \mathbf{A}_0}{\partial t} = n_b \mathbf{j}_0 \times S_\omega{}^{-1}, \tag{5}$$

where $n_b \mathbf{j}_0$ is the non-perturbed eddy-current in V_b obtained from the base field $\mathbf{A}_0$ (2). This equation shows that the first order perturbation of the vector potential due to a non-conducting inclusion is simply governed by the induced base field at the location of the inclusion. However, this perturbation is not damped by a diffusion-induction mechanism and does not generate eddy-current. To take into account induction, it should be necessary to consider the second order of $\mathbf{A}_\alpha$ perturbation. The electrical current is zero in the inclusion, and the spatial distribution of $\mathbf{j}_0$ around the inclusion is modified in $\mathbf{j}_0 + S_\omega \mathbf{j}_\alpha^1$, where $\mathbf{j}_\alpha^1 = \frac{\partial \mathbf{A}_\alpha^1}{\partial t} \times -S_\omega$. Consequently, we expect an increase of dissipation in a thin layer surrounding the inclusion. Finally, in Eq. (5), $n_b \mathbf{j}_0$ is understood as the source term of the Poisson equation. Note that, at the first order of S_ω, the total electrical current density still respects the conservation equation in

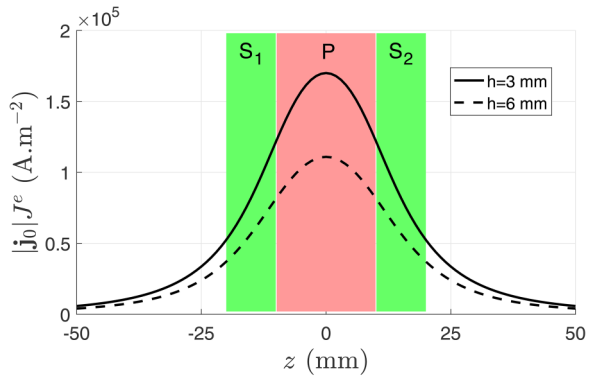

FIG. 2. Evolution of the dimensional unperturbed current density with the axial position for two inclusion depths, as obtained from Eqs. (2) and (3). $R = 12.5\,\text{mm}$, $\omega = 2\pi \times 1000\,\text{rad}\,\text{s}^{-1}$, $I^e = 0.17\,\text{A}$. The zones P, S1, and S2 denote the primary and secondary coil positions.

the whole volume and its normal component at the inclusion boundary is $\mathcal{O}(S_\omega^2) \ll 1$.

The solution of Eq. (5) is

$$\mathbf{A}_\alpha^1(\mathbf{r}) \times S_\omega = -\frac{1}{4\pi}\int_{V_b} \frac{\mathbf{j_0}(\mathbf{r}')}{|\mathbf{r}-\mathbf{r}'|}\, dV(\mathbf{r}'). \tag{6}$$

The perturbation of the vector potential is obtained from the distribution of the non-perturbed eddy-current field $\mathbf{j}_0$ at the location of the inclusion. A similar approach is developed in order to analyze the perturbation of the Lorentz force due to an insulating defect in a conducting medium.[15] An example of $|\mathbf{j}_0|(z)$, where z is the axial coordinate, is displayed in Fig. 2 for two different depths h and for a given pulsation. Here, the non-perturbed current density $|\mathbf{j}_0|$ is given in SI units. As expected, $|\mathbf{j}_0(z)|$ is maximum at the center of the P coil for both depths and decreases by a factor ~ 2 at the center of the two S coils. We note that the major part of the electromagnetic energy is localized in the liquid metal just under the three coils. As the liquid metal flows, the inclusion crosses the ECFM and sees the $\mathbf{j}_0$ distribution corresponding to its depth position. Then, the ECFM monitors the perturbation of the eddy-currents during the inclusion displacement.

III. EXPERIMENTAL SETUP

In order to validate the perturbation model for one inclusion, we design a specific experimental setup with an ECFM as depicted in Fig. 1. The three coils have the same radius $R_S = 35\,\text{mm}$ and a length of 20 mm (P) and 10 mm (S1 and S2). For all the experiments, the phase and intensity of $\mathbf{j}^e$ are imposed using a transconductance amplifier. The ECFM is translated at a constant velocity U varying between 1 and $10^3\,\text{mm/s}$ ($Re_m \leq 0.025$), around a ceramic tube (Macor™) containing a static liquid metal (galinstan GaInSn, $\sigma = 3.46 \times 10^6\,\text{S/m}$, diameter $2R = 25\,\text{mm}$). The non-conducting inclusion is a polymer bead (Visijet® M3 Crystal) of various radii ($R_b = 1$, 1.5, 2, and 2.5 mm) made by 3D printing (3D Systems ProJet 3500 HD with a precision of $\pm 0.025\,\text{mm}$). The beads are fixed at different depths ($h = 3$ and 6 $\pm 0.25\,\text{mm}$) with a thin thread of diameter $50\,\mu\text{m}$ (Fig. 3). The perturbation of the voltage difference between S1 and S2 caused by the inclusion, ΔV_α, is obtained by demodulation of the AC voltage signal using a lock-in amplifier (HF2LI-MF Zurich Instruments). The values of ΔV_α are then averaged over ten acquisitions with a standard deviation of $\sim 2\,\mu\text{V}$. We observe that the measured signal is sensitive to the presence of the inclusion for the whole ranges of frequency (between 5×10^2 and $2 \times 10^4\,\text{Hz}$), inclusion size R_b, and position h. The study in frequency points out that the model is valid only at low frequencies, typically between 5×10^2 and $2 \times 10^3\,\text{Hz}$, in agreement with the model hypothesis. In this frequency range, the skin depth varies between 12.1 and 6.1 mm. With these values, we find $S_\omega/Re_m \geq 3$ and $S_\omega \leq 0.3$; hence, the assumption $Re_m \ll S_\omega \ll 1$ is verified except for large beads and high frequencies.

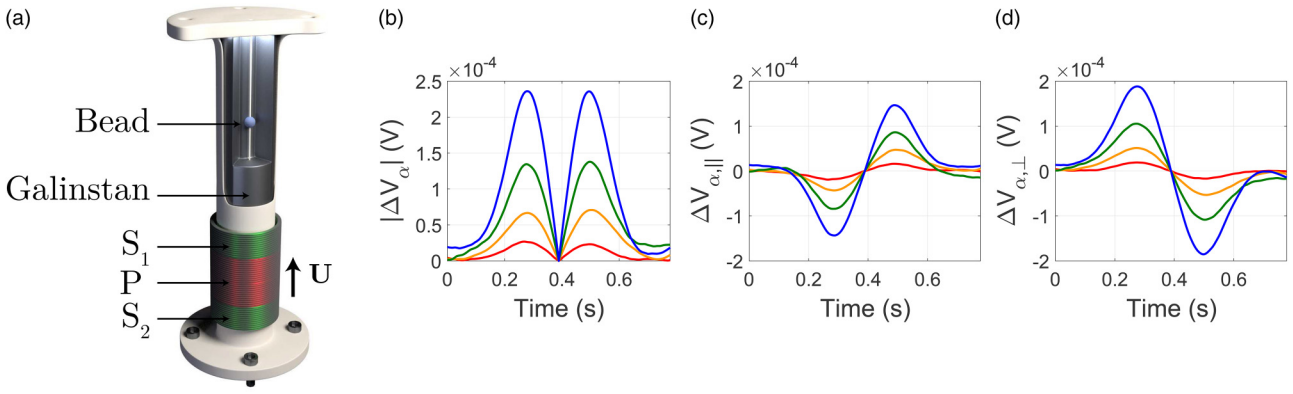

FIG. 3. (a) Experimental ECFM (S1-P-S2) device in translation at constant velocity U around the tube of galinstan. (b)–(d) Modulus, in-phase, and in-quadrature components of ΔV_α for different bead diameters (red curves 2 mm, yellow curves 3 mm, green curves 4 mm, blue curves 5 mm). Bead distance to the wall $h = 3\,\text{mm}$. Frequency 1000 Hz. Translation velocity $U = 100\,\text{mm}\,\text{s}^{-1}$.

Figure 3 depicts the demodulated signals of ΔV_α (modulus, in-phase, and in-quadrature components with respect to the phase reference of $\mathbf{j}^e$), versus the transit time of the bead through the ECFM, for various R_b (here, U, ω, and h are fixed). We recall that the existence of both in-phase and in-quadrature components is a direct consequence of the phase shift of the base field $\mathbf{A}_0$ [Eqs. (2) and (3)]. The curves present two extrema located approximately at the limits between the primary and the secondary coils. When the bead is at the middle of P, ΔV_α is zero. Furthermore, the signal amplitude increases by one decade when R_b changes from 1 to 2.5 mm. This last result shows that the ECFM device is very sensitive to the bead volume. In addition, as observed previously, all the experiments confirm that ΔV_α is independent of U at small Re_m.[3,4]

IV. RESULTS AND DISCUSSION

By applying the Faraday law on the perturbed potential $\mathbf{A}^1_\alpha$ in Eq. (6), one can predict the dimensional induced voltage difference ΔV_α

$$\frac{\Delta V_\alpha}{\mu_0 \omega J^e R_b^3} = \sum_{N_S} \frac{d}{dt}\left\{ \oint_{S_2} \mathbf{A}^1_\alpha \cdot d\mathbf{r} - \oint_{S_1} \mathbf{A}^1_\alpha \cdot d\mathbf{r} \right\}, \tag{7}$$

where the contour integrals correspond to 1 turn of S1 and S2 and N_S is the number of turns of the two secondary coils. Figure 4 compares the model and experiments for two bead positions, $h = 3$ and 6 mm, with $R_b = 1.5$ mm, at 1000 Hz. The exact solutions of Eqs. (5) and (6) are compared with an approximated solution of $\mathbf{A}^1_\alpha$ in which $\mathbf{j}_0(\mathbf{r}') \approx$ cst in Eq. (6). In this approximation, the value of $\mathbf{j}_0(\mathbf{r}')$ is taken at the location of the inclusion center. The uncertainties on the geometrical parameters R, R_b, and h are an important cause of deviation between the theoretical and experimental values of $|\Delta V_\alpha|$. Within the limit of the measurement uncertainties, we observe a good agreement between the experiments and the model, for both exact and approximated solutions. The experimental results in Figs. 3 and 4 exhibit a slight dissymmetry of the two $|\Delta V_\alpha|$ peaks due to the accuracy of the physical parameters mentioned above responsible for the uncertainty of the experimental $\Delta V_\alpha = 0$ line position.

As expected from the assumptions of the model ($S_\omega \ll 1$), we find that the model deviates from the experimental results for a large bead radius ($R_b > 2$ mm) and a high frequency (over 2000 Hz). Henceforth, the hypothesis of a current density $\mathbf{j}_0$ uniformly distributed in V_b gives a very good approximation of ΔV_α. Within this assumption, Eq. (6) simply becomes $\mathbf{A}^1_\alpha(\mathbf{r}) \approx -\frac{\mathbf{j}_0}{3|\mathbf{r}|}$, where $\mathbf{r}$ is now the vector position in the whole space from the inclusion center. For one turn of S1 or S2, the circulation of $\mathbf{A}^1_\alpha$ in Eq. (7) is then

$$\oint \mathbf{A}^1_\alpha \cdot d\mathbf{r} \approx \frac{\Lambda}{6}|\mathbf{j}_0|\left\{2E(\pi, m) + (m^2 - 2)F(\pi, m)\right\}, \tag{8}$$

where $F(\pi, m)$ and $E(\pi, m)$ are the complete elliptic integrals of the first and second kind,[14] with $m^2 = \frac{4R_S}{\rho\Lambda^2}$ and $\Lambda^2 = \left[(R_S + \rho)^2 + \xi^2\right]/\rho^2$. The radial position of the bead center in the tube is $\rho = R - h$, and the axial distance between the bead center and the plane containing the coil turn is ξ. Incorporating Eq. (8) in Eq. (7), the right-hand side of Eq. (7) is a function of ω, h, and z. Note that the ω dependence is contained only in $|\mathbf{j}_0|$.

We define $\Delta V^\star_\alpha$ as the maximum value of ΔV_α reached when the z-position of the bead is approximately at the limit between the primary and the secondary coils. At this position, we introduce the parameter $\Upsilon_\alpha = \Delta V^\star_\alpha / \mu_0 \omega J^e = R_b^3 f_\omega(h)$, where the dimensionless function $f_\omega(h)$ is the maximum value of the sum in Eq. (7). Figure 5 displays $f_\omega(h)$ for the geometry of our experimental setup at different frequencies. It is seen that the function $f_\omega(h)$ decreases

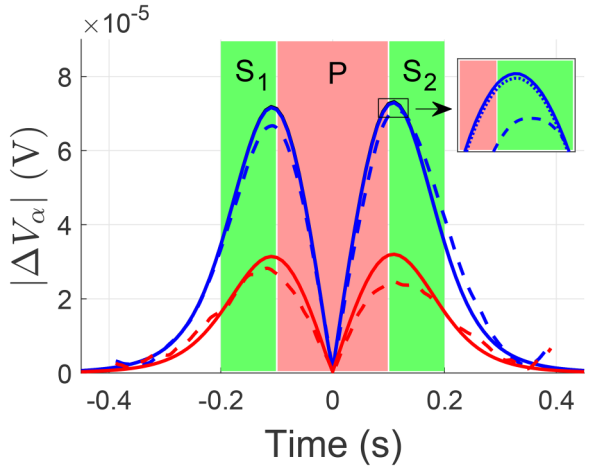

FIG. 4. Comparison between the model (continuous lines) and experiments (dashed lines): modulus of ΔV_α versus time for a 3 mm bead diameter at two different depths: $h = 3$ mm blue curves and $h = 6$ mm red curves. Frequency 1000 Hz, translation velocity $U = 100$ mm s^{-1}. Inlet: zoom of the model solutions (continuous line: uniform distribution of $\mathbf{j}_0$, dotted line: exact solutions).

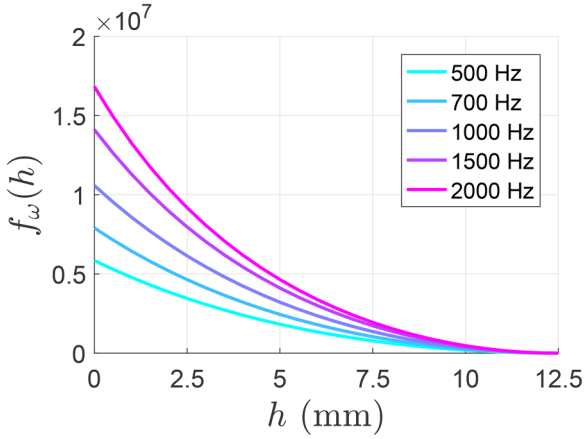

FIG. 5. Graph of the function $f_\omega(h)$ from Eqs. (7) and (8) for various frequencies.

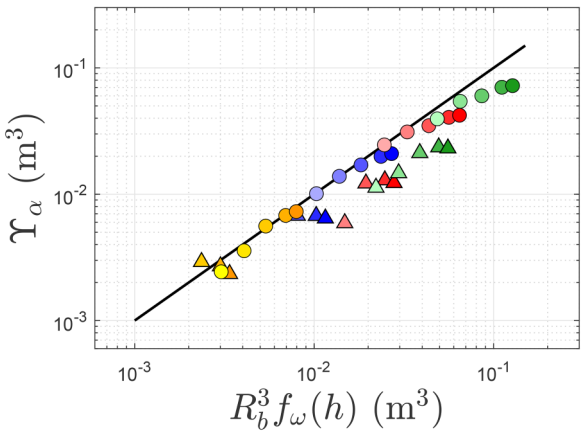

FIG. 6. Master curve $\Upsilon_\alpha = \Delta V_\alpha^\star / \mu_0 \omega J^e$ versus $R_b^3 f_\omega(h)$. Comparison between the model (continuous line) and experiments (points) for various R_b: 1 mm (yellow), 1.5 mm (blue), 2 mm (red), and 2.5 mm (green). The bead depth is depicted by circles ($h = 3$ mm) and triangles ($h = 6$ mm). For each bead, the color lightness corresponds to the AC frequency of the measurements, from light (500 Hz) to dark (2000 Hz).

with h and vanishes at the center of the tube ($h = R$), where $\mathbf{j}_0 = \mathbf{0}$. Figure 6 compares the theoretical values of Υ_α predicted by the model with those of experiments. For $h = 3$ mm, the measurements correctly follow the relation $\Upsilon_\alpha = R_b^3 f_\omega(h)$. On the other hand, for $h = 6$ mm, the measurements slightly deviate from the previous relation. For a fixed bead depth h, an increase in frequency or bead volume also leads to a deviation of the experimental data from the model prediction. Indeed, as R_b, h, and ω increase, the induction term $nS_\omega \partial \mathbf{A}_\alpha / \partial t$ in Eq. (4) becomes non-negligible compared with the Laplacian term $\nabla^2 \mathbf{A}_\alpha$. In this case, the eddy-current perturbation is responsible for a spatial decay of $\mathbf{A}_\alpha$, resulting in a lower value of ΔV_α. As a consequence, the model overestimates Υ_α for high R_b, h, and ω and gives an upper limit of the experimental data.

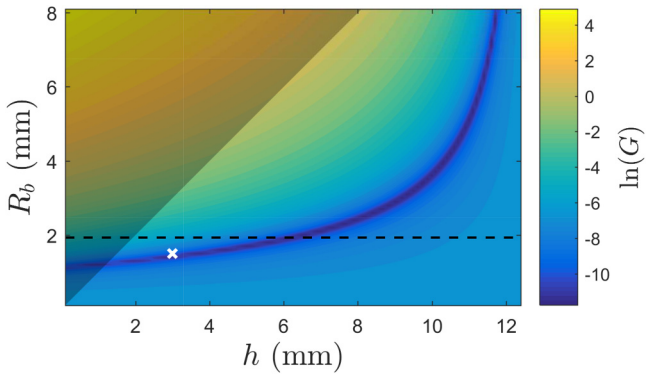

FIG. 7. Contour of the objective function $G(h, R_b) = \sum_i \left[\Upsilon_{\alpha,i}^{\text{exp}} - \Upsilon_{\alpha,i}^{\text{th}}(h, R_b) \right]^2$, where the i index corresponds to the AC frequency ω_i. The cross indicates the experimental value of (R_b, h). The shaded zone corresponds to $R_b > h$, and the dashed line depicts the limit of the model assumption $S_\omega = 0.1$ for a frequency of 2000 Hz.

Finally, if one wants to determine R_b and h from experiments by the inverse method, one can show that R_b and h are linked by a unique relation obtained by least squares minimization of the difference between experimental and theoretical ΔV_α at various ω. This property results from the self-similarity in R_b^3 and h of the solutions of the model. As an example, Fig. 7 displays the curve of this relation in the contour graph of the objective function for the experimental data obtained with $R_b = 1.5$ mm and $h = 3$ mm. We observe that the experimental (R_b, h) value belongs to the minimum $R_b - h$ curve within the limit of the model assumption ($S_\omega \ll 1$) and the geometrical constraint ($R_b < h$). Hence, a reasonable estimation of R_b can be determined from "blind" measurements of ΔV_α at different frequencies, but the value of R_b can be characterized precisely if h is known.

V. CONCLUSION

In this article, we have presented a perturbation model of the vector potential due to a non-conducting inclusion in a liquid metal flow. The perturbation is calculated from the solution of the unperturbed current density $\mathbf{j}_0$ taken at the center of the inclusion and distributed all over the inclusion volume. The main assumption of the model is $Re_m \ll S_\omega \ll 1$, corresponding to small values of R_b, h, and ω. We designed a specific experimental setup in order to validate the model and we observed a good agreement within the limit of the hypothesis. An inverse approach shows that a good order of magnitude of R_b can be determined from experiments at various frequencies. This work points out that inductive effects should be taken into account for the study of two-phase liquid metal flows at higher frequencies. Finally, this model could be extended to calculate the response of a distribution of dilute inclusions. The approach developed in this article will be of direct interest for the detection of bubbles in the metallurgy process and in nuclear safety design for sodium-cooled fast reactors.

ACKNOWLEDGMENTS

The authors acknowledge G. Ehses at IMFT Toulouse for his technical assistance. This work has been financially supported by CEA Cadarache.

REFERENCES

[1] N. Terzija, W. Yin, G. Gerbeth, F. Stefani, K. Timmel, T. Wondrak, and A. Peyton, Meas. Sci. Technol. **22**, 015501 (2011).
[2] R. Moreau, Z. Tao, and X. Wang, Appl. Phys. Lett. **109**, 024104 (2016).
[3] M. Kumar, Ph. Tordjeman, W. Bergez, and M. Cavaro, Rev. Sci. Instrum. **86** (10), 106104 (2015).
[4] M. Kumar, W. Bergez, Ph. Tordjeman, R. Arinero, and K. Paumel, J. Appl. Phys. **119**, 185105 (2016).
[5] J. C. Maxwell, *A Treatise on Electricity and Magnetism* (Dover Publications, New York, 1954).
[6] J. R. Bowler, S. A. Jenkins, L. D. Sabbagh, and H. A. Sabbagh, J. Appl. Phys. **70**, 1107 (1991).
[7] S. Schwarz and J. Fröhlich, Int. J. Multiphas. Flow **62**, 134 (2014).
[8] J. Zhang, M.-J. Ni, and R. Moreau, Phys. Fluids **28**, 032101 (2016).

[9]Z. Lyu, T. Boeck, C. Karcher, and A. Thess, Magnetohydrodynamics **53**, 653 (2017).
[10]J. A. Shercliff, *The Theory of Electromagnetic Flow-Measurement* (Cambridge University Press, Cambridge, 1962).
[11]R. Moreau, *Magnetohydrodynamics* (Kluwer Academic Publishers, Dordrecht, 1990).
[12]C. Dodd and W. Deeds, J. Appl. Phys. **39**(6), 2829 (1968).
[13]M. Hirayama, IEEE Trans. Nucl. Sci. **24**(5), 2021–2030 (1977).
[14]M. Abramowitz and I. Stegun, *Handbook of Mathematical Functions* (Dover Publications, New York, 1964).
[15]E.-M. Dolker, R. Schmidt, K. Weise, B. Petkovic, M. Ziolowski, H. Brauer, and J. Haueisen, IEEE Trans. Magn. **54**, 6200105 (2018).